Inorganic Chemistry

Article

pubs.acs.org/IC

# Straightforward Reductive Routes to Air-Stable Uranium(III) and Neptunium(III) Materials

Justin N. Cross,[†,‡] Eric M. Villa,[⊥] Victoria R. Darling,[‡] Matthew J. Polinski,[†] Jian Lin,[†,‡] Xiaoyan Tan,[†] Naoki Kikugawa,[§] Michael Shatruk,[†] Ryan Baumbach,[§] and Thomas E. Albrecht-Schmitt*[,†]

[†]Department of Chemistry and Biochemistry, Florida State University, 95 Chieftan Way, 310 DLC, Tallahassee, Florida 32306-4390, United States

[‡]Department of Chemistry and Biochemistry, University of Notre Dame, 156 Fitzpatrick Hall, Notre Dame, Indiana 46556 United States

[§]National High Magnetic Field Laboratory, Florida State University, Tallahassee, Florida 32310, United States

[⊥]Department of Chemistry, Creighton University, 2500 California Plaza, Omaha, Nebraska 68178, United States

Supporting Information

**ABSTRACT:** Studies of trivalent uranium ($U^{3+}$) and neptunium ($Np^{3+}$) are restricted by the tendency of these ions to oxidize in the presence of air and water, requiring manipulations to be carried out in inert conditions to produce trivalent products. While the organometallic and high-temperature reduction chemistry of $U^{3+}$ and, to a much smaller extent, $Np^{3+}$ has been explored, the study of the oxoanion chemistry of these species has been limited despite their interesting optical and magnetic properties. We report the synthesis of $U^{3+}$ and $Np^{3+}$ sulfates by utilizing zinc amalgam as an *in situ* reductant with absolutely no regard to the exclusion of $O_2$ or water. By employing this method we have developed a family of alkali metal $U^{3+}$ and $Np^{3+}$ sulfates that are air and water stable. The structures, electronic spectra, and magnetic behavior are reported.

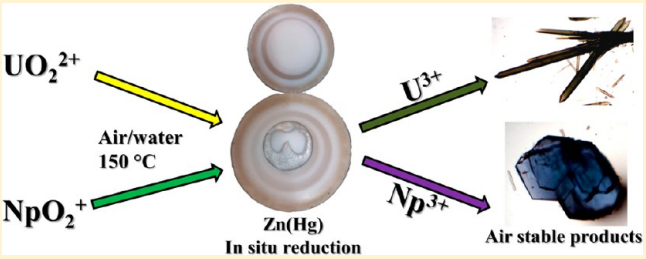


## INTRODUCTION

Carefully controlling, manipulating, and stabilizing different oxidation states in aqueous solutions and the solid state are some of the major facets of actinide chemistry. Uranium and neptunium can both adopt a wide variety of oxidation states (+3 to +6 with the addition of +7 for Np). However, the dominant species that have been explored are the hexavalent uranyl ($UO_2^{2+}$) and pentavalent neptunyl ($NpO_2^{+}$) units.[1−6] The least-explored oxidation state of both U and Np in aqueous media is, by far, the trivalent state (although a reliable report of a highly reactive $U^{2+}$ complex has recently emerged).[7,8] This is especially true when looking at the solid-state oxyanion chemistries of these elements.[9−11] This deficit is not due to any lack of interesting properties; $U^{3+}$ was one of the first lasing mediums and inherently acts as a single molecule magnet.[12−16] Additionally, $U^{3+}$ and $Np^{3+}$ have the ability to form significant covalent bonds that could lead to significant bonding differences between these species and their lanthanide congeners.[15−17] Rather, the lack of $U^{3+}$ and $Np^{3+}$ complexes arises from their propensity to oxidize quickly in the presence of air and water.[10,11,20,21]

This restriction has caused the bulk of the work on these trivalent species to be done in rigorous air-free conditions and to be more organometallic in nature where it was found that some $U^{3+}$ complexes can be an effective catalyst.[22−29] $U^{3+}$ can also be synthesized at higher temperatures using a strongly reducing atmosphere.[18,19] This method has been used to produce materials for intricate studies into the optical properties of $U^{3+}$.[30] It has been shown that under inert air conditions aqueous solutions of $U^{3+}$ and $Np^{3+}$ can be produced electrochemically or by zinc amalgam.[31] This technique was used to produce the hydrated trihalides, formate, a variety of sulfate complexes, and most recently the aquo triflate series.[32−39] The $U^{3+}$ sulfate complexes have the general formula $AU(SO_4)_2{\cdot}XH_2O$ (A = $NH_4^+$, $Na^+$, $K^+$, $Rb^+$, $Cs^+$) or $U_2(SO_4)_3{\cdot}8H_2O$. These were synthesized under low-temperature inert-atmosphere conditions producing marginally air-stable products, and while the reflectance spectra and magnetic susceptibilities were reported, the only crystal structure published from all of these sulfate compounds is that of $NH_4U(SO_4)_2{\cdot}4H_2O$.[40] A number of $Np^{3+}$ solid compounds have been synthesized from aqueous solutions using rongalite ($NaHOCH_2SO_2$) as a reductant and stabilizing agent, but very little information was reported on the physical properties of these compounds.[41−43]

We recently explored the *in situ* reduction of hexavalent $AnO_2^{2+}$ or pentavalent $AnO_2^{+}$ to tetravalent $An^{4+}$ complexes hydrothermally.[44−47] Reduction here is driven either by

**Received:** April 4, 2014
**Published:** June 25, 2014

   dx.doi.org/10.1021/ic500771t | *Inorg. Chem.* 2014, 53, 7455−7466

solubility (i.e., the much greater insolubility of 4+ makes reduction more favorable) or by using the reducing phosphite ligand. Of particular interest were the phosphite studies showing the control over reduction by adjusting time and pH, yielding partially reduced and fully reduced $U^{4+}$ species. This study represents one of the only systematic explorations of *in situ* hydrothermal reduction.[46,47] There have been a few other examples of *in situ* hydrothermal reduction using a variety of reducing agents and metals.[48−58] Note that these studies were unable to access oxidation states that have negative reduction potentials versus normal hydrogen electrode (NHE).

While exploring the solid-state chemistry of lower-valent uranium by combining zinc amalgam with hydrothermal reaction techniques we were able to isolate a family of $U^{3+}$ sulfates. These compounds were produced with absolutely no exclusion of air from a hexavalent uranium source, $UO_2(CH_3COOH)_2{\cdot}2H_2O$, alkali metal carbonates (A = Na, K, Rb, Cs), and $H_2SO_4$. The reagents were loaded into an autoclave along with a chunk of zinc amalgam and then heated as is. After isolation of $U^{3+}$ products was realized, similar reactions were carried out using a pentavalent Np source, $NpO_2OH$, and the alkali metal carbonates, whereupon five $Np^{3+}$ products were synthesized. The products were analyzed by single-crystal optical spectroscopy and single-crystal X-ray crystallography. For $NaU(SO_4)_2(H_2O)$, $K_5U_2(SO_4)_6H_2O$, and $CsNp(SO_4)_2$ enough product was available to further characterize the materials by magnetic susceptibility.

## EXPERIMENTAL SECTION

**Syntheses.** Zn shot (99.9% Alfa Aesar), Hg (99.9% Alfa Aesar), $UO_2(CH_3COO)_2{\cdot}2H_2O$ (99% Fisher), $Na_2CO_3$ (ACS Reagent grade, Matheson Coleman Bell), $K_2CO_3$ (99.9% Alfa Aesar), $Rb_2CO_3$ (99.9% Alfa Aesar), $Cs_2CO_3$ (99.9% Alfa Aesar), and $H_2SO_4$ (98% Alfa Aesar) were all used as obtained. A sample of $^{237}Np(V)$ hydroxide was prepared by first digesting $NpO_2$ (Oak Ridge 99.9%) in 8 M $HNO_3$ for 3 d at 200 °C (in an autoclave). The solution was reduced to a moist residue and redissolved in water, forming a neptunium(VI) nitrate solution. A large excess of $NaNO_2$, followed by an excess of $NH_4OH$, was added to this solution, resulting in the precipitation of neptunium(V) hydroxide. The precipitate was then filtered and dried at 120 °C for about 30 min. The $NpO_2OH$ was then used as obtained. Reactions were run in PTFE-lined Parr 4749 autoclaves with a 23 mL internal volume for uranium and with a 10 mL internal volume autoclave for neptunium. Deionized water was used in all reactions. Zn amalgam was prepared by mixing an approximate ratio by weight of 30%:70% Zn/Hg in a glass vial. Typical amounts are 2.20 g Zn and 4.8 g of Hg. The vial was then heated on a hot plate until the Zn completely dissolved into the Hg. The molten amalgam was then carefully poured into the Teflon liner of a Parr 4749 autoclave with a 23 mL or 10 mL internal volume (see Supporting Information, Figure S1). Reactants were then loaded into the liners with the amalgam. Amalgams were recovered after reactions and reused in subsequent reactions. Amalgams can be reused in 10 to 15 reactions before losing enough Zn to render them unusable. ***Caution!*** *While the $UO_2(CH_3COO)_2{\cdot}2H_2O$ used in this study contained depleted uranium, standard precautions for handling radioactive materials should be followed. $^{237}Np$ ($t_{1/2}$ = 2 144 000 y) represents serious health risks owing to its α and γ emission. All studies with neptunium were conducted in a laboratory dedicated to studies on transuranium elements. This laboratory is located in a nuclear science facility and is equipped with high-efficiency particulate air (HEPA) filtered hoods and negative-pressure gloveboxes that are ported directly into the hoods. A series of counters continually monitor radiation levels in the laboratory. The laboratory is licensed by the Nuclear Regulatory Commission. All experiments were carried out with approved safety operating procedures. All free-flowing solids are worked within gloveboxes, and products are only examined when coated with either water or Krytox oil and water. There are significant limitations in accurately determining yield with neptunium compounds because this requires drying, isolating, and weighing a solid, which poses certain risks, as well as manipulation difficulties given the small quantities employed in the reactions.*

*$NaU(SO_4)_2(H_2O)$.* $UO_2(CH_3COO)_2{\cdot}2H_2O$ (0.200 mmol, 0.0848 g), $Na_2CO_3$ (0.600 mmol, 0.0636 g), $H_2SO_4$ (2.0 mmol, 220 μL, 98%), and 1.8 mL of $H_2O$ were loaded into an autoclave with Zn amalgam, sealed, and heated to 150 °C for 2 h, then cooled to 25 °C at 5 °C/h. The product was rinsed with water, and prism-shaped crystals, which were green under fluorescent lights and tobacco-colored under lamp light, were isolated. Estimated yield ∼50% based on U. Product was the same if reaction time was increased to 12 h.

*$K_5U_2(SO_4)_6(H_2O)$.* $UO_2(CH_3COO)_2{\cdot}2H_2O$ (0.200 mmol, 0.0848 g), $K_2CO_3$ (0.600 mmol, 0.0827 g), $H_2SO_4$ (2.0 mmol, 220 μL, 98%), and 1.8 mL of $H_2O$ were loaded into an autoclave with Zn amalgam, sealed, and heated to 150 °C for 2 h, then cooled to 25 °C at 5 °C/h. The products were rinsed with water, and block-shaped crystals, which were black under fluorescent light and gold-colored under lamp light, were isolated along with a green U(IV) sulfate. Estimated yield of the two products was ∼80% with approximately equal amounts of U(III) and U(IV). Increasing the reaction time increased the amount of $K_5U_2(SO_4)_6(H_2O)$, but beyond 12 h the amount decreased significantly.

*$RbU(SO_4)_2(H_2O)$.* $UO_2(CH_3COO)_2{\cdot}2H_2O$ (0.200 mmol, 0.0848 g), $Rb_2CO_3$ (0.600 mmol, 0.1379 g), $H_2SO_4$ (2.0 mmol, 220 μL, 98%), and 1.8 mL of $H_2O$ were loaded into an autoclave with Zn amalgam, sealed, and heated to 150 °C for 2 h, then cooled to 25 °C at 5 °C/h. The products were rinsed with water, and gold plates were isolated along with a green U(IV) sulfate. Estimated yield of the two products is ∼80%. Only a small amount of the gold plates was isolated after 2 h. A relationship similar to the formation of $K_5U_2(SO4)_6(H_2O)$ with time was found with $RbU(SO_4)_2(H_2O)$.

*$CsU(SO_4)_2(H_2O)$.* $UO_2(CH_3COO)_2{\cdot}2H_2O$ (0.200 mmol, 0.0848 g), $Cs_2CO_3$ (0.600 mmol, 0.1955 g), $H_2SO_4$ (2.0 mmol 220 μL 98%), and 1.8 mL of $H_2O$ were loaded into an autoclave with Zn amalgam, sealed, and heated to 150 °C for 2 h, then cooled to 25 °C at 5 °C/h. The products were rinsed with water, and gold plates were isolated along with a green U(IV) sulfate. Estimated yield of the two products is ∼80%. Only a small amount of the gold plates was isolated after 2 h. A relationship similar to the formation of $K_5U_2(SO_4)_6(H_2O)$ with time was found with $CsU(SO_4)_2(H_2O)$.

*$NaNp(SO_4)_2(H_2O)$.* $NpO_2OH$ (0.0290 mmol, 0.0083 g), $Na_2CO_3$ (0.087 mmol, 0.0092 g), $H_2SO_4$ (0.576 mmol, 32 μL, 98%), and 170 μL of $H_2O$ were loaded into an autoclave with Zn amalgam, sealed, and heated to 150 °C for 2 h, then cooled to 25 °C at 5 °C/h. The product was rinsed with water, and prism-shaped crystals, which were blue under fluorescent lights and purple under lamp light, were isolated.

*$KNp(SO_4)_2(H_2O)$ and $KNp(SO_4)_2$.* $NpO_2OH$ (0.0168 mmol, 0.0048 g), $K_2CO_3$ (0.050 mmol, 0.0070 g), $H_2SO_4$ (0.336 mmol, 20 μL 98%), and 180 μL of $H_2O$ were loaded into an autoclave with Zn amalgam, sealed, and heated to 150 °C for 2 h, then cooled to 25 °C at 5 °C/h. The product was rinsed with water, and two types of crystals were isolated. Thin prism-shaped crystals ($KNp(SO_4)_2(H_2O)$), which were blue under fluorescent lights and purple under lamp light, along with darker, similarly colored block crystals ($KNp(SO_4)_2$), were obtained.

*$RbNp(SO_4)_2$.* $NpO_2OH$ (0.0206 mmol, 0.0059 g), $Rb_2CO_3$ (0.0618 mmol, 0.0142 g), $H_2SO_4$ (0.412 mmol, 23 μL, 98%), and 175 μL of $H_2O$ were loaded into an autoclave with Zn amalgam, sealed, and heated to 150 °C for 2 h, then cooled to 25 °C at 5 °C/h. The product was rinsed with water, and plates, which were blue under fluorescent lights and purple under lamp light, were isolated.

*$CsNp(SO_4)_2$.* $NpO_2OH$ (0.0315 mmol, 0.0090 g), $Cs_2CO_3$ (0.0945 mmol, 0.0182 g), $H_2SO_4$ (0.630 mmol, 35 μL 98%), and 165 μL of $H_2O$ were loaded into an autoclave with Zn amalgam, sealed, and heated to 150 °C for 2 h, then cooled to 25 °C at 5 °C/h. The product was rinsed with water, and hexagonal-shaped plates, which were blue under fluorescent lights and purple under lamp light, were isolated.

**Crystallographic Studies.** Single crystals of the above compounds were mounted on cryoloops with viscous Krytox and optically aligned on a Bruker APEXII Quazar X-ray diffractometer using a digital camera. Initial intensity measurements were performed using an IμS X-ray microsource (Mo Kα, λ = 0.710 73 Å) with high-brilliance and high-


dx.doi.org/10.1021/ic500771t | Inorg. Chem. 2014, 53, 7455−7466

**Table 1. Crystallographic Information for U Compounds**

| compound | $NaU(SO_4)_2(H_2O)$ | $K_5U_2(SO_4)_6(H_2O)$ | $RbU(SO_4)_2$ | $CsU(SO_4)_2$ |
|---|---|---|---|---|
| formula mass | 471.16 | 1263.92 | 515.62 | 563.06 |
| color and habit | olive, prism | dark yellow, block | gold, plate | gold, plate |
| space group | $P3_22_1$ | $C2/c$ | $P6_3/mmc$ | $P2_1/n$ |
| $a$ (Å) | 7.0282(3) | 17.740(1) | 5.377(4) | 7.871(2) |
| $b$ (Å) | 7.0282(3) | 7.0516(6) | 5.377(4) | 5.464(1) |
| $c$ (Å) | 12.9377(6) | 19.464(1) | 13.99(1) | 17.044(3) |
| $a$ (deg) | 90 | 90 | 90 | 90 |
| $\beta$ (deg) | 90 | 112.300(1) | 90 | 91.425(2) |
| $\gamma$ (deg) | 120 | 90 | 120 | 90 |
| $V$ (Å$^3$) | 553.45 | 2252.83(3) | 350.2(4) | 732.9(3) |
| $Z$ | 3 | 4 | 2 | 4 |
| $T$ (K) | 296 | 296 | 296 | 100 |
| $\lambda$ (Å) | 0.710 73 | 0.710 73 | 0.710 73 | 0.710 73 |
| maximum 2Θ (deg) | 30.52 | 27.53 | 27.70 | 27.51 |
| $\rho_{calcd}$ (g cm$^{-3}$) | 4.241 | 3.727 | 4.889 | 5.103 |
| $\mu$(Mo K$\alpha$) (cm$^{-1}$) | 226.44 | 159.54 | 306.78 | 276.19 |
| $R(F)$ for $F_0^2 > 2s(F_0^2)^a$ | 0.0138 | 0.0256 | 0.0498 | 0.0244 |
| $R_w(F_0^2)^b$ | 0.0326 | 0.0552 | 0.0932 | 0.0528 |

$^aR(F) = \Sigma||F_0| - |F_c||/\Sigma|F_0|$. $^bR_w(F_0^2) = [\Sigma[w(F_0^2 - F_c^2)^2]/\Sigma wF_0^4]^{1/2}$.

**Table 2. Selected Bond Distances for U Compounds**

| $NaU(SO_4)_2(H_2O)$ | | $K_5U_2(SO_4)_6(H_2O)$ | | $RbU(SO_4)_2$ | | $CsU(SO_4)_2$ | |
|---|---|---|---|---|---|---|---|
| U(1)−O(1) | 2.492(3) | U(1)−O(8) | 2.392(4) | U(1)−O(2) | 2.50(1) | U(1)−O(8) | 2.460(7) |
| U(1)−O(1)′ | 2.492(3) | U(1)−O(3) | 2.436(4) | U(1)−O(2) | 2.50(1) | U(1)−O(4) | 2.478(6) |
| U(1)−O(4) | 2.504(3) | U(1)−O(7) | 2.449(4) | U(1)−O(2) | 2.50(1) | U(1)−O(6) | 2.520(6) |
| U(1)−O(4)′ | 2.504(3) | U(1)−O(1) | 2.452(4) | U(1)−O(2) | 2.50(1) | U(1)−O(7) | 2.526(7) |
| U(1)−O(5) | 2.535(6) | U(1)−O(2) | 2.466(4) | U(1)−O(2) | 2.50(1) | U(1)−O(3) | 2.527(6) |
| U(1)−O(3) | 2.586(2) | U(1)−O(4) | 2.488(5) | U(1)−O(2) | 2.50(1) | U(1)−O(5) | 2.574(6) |
| U(1)−O(3)′ | 2.586(2) | U(1)−O(5) | 2.501(4) | S(1)−O(2) | 1.45(1) | U(1)−O(2) | 2.575(6) |
| U(1)−O(2) | 2.588(2) | U(1)−O(6) | 2.555(4) | S(1)−O(2) | 1.450(9) | U(1)−O(1) | 2.710(7) |
| U(1)−O(2)′ | 2.588(2) | U(1)−O(7)′ | 2.610(4) | S(1)−O(2) | 1.45(1) | U(1)−O(1) | 2.761(7) |
| S(1)−O(1) | 1.461(3) | S(1)−O(13) | 1.440(4) | S(1)−O(1) | 1.45(2) | S(1)−O(2) | 1.473(7) |
| S(1)−O(4) | 1.465(3) | S(1)−O(12) | 1.443(4) | | | S(1)−O(4) | 1.476(7) |
| S(1)−O(2) | 1.479(3) | S(1)−O(3) | 1.491(4) | | | S(1)−O(5) | 1.482(6) |
| S(1)−O(3) | 1.480(3) | S(1)−O(7) | 1.515(4) | | | S(1)−O(8) | 1.484(7) |
| | | S(2)−O(11) | 1.441(4) | | | S(2)−O(6) | 1.469(6) |
| | | S(2)−O(4) | 1.472(4) | | | S(2)−O(7) | 1.478(7) |
| | | S(2)−O(1) | 1.487(4) | | | S(2)−O(3) | 1.479(6) |
| | | S(2)−O(8) | 1.493(4) | | | S(2)−O(1) | 1.503(6) |
| | | S(3)−O(10) | 1.439(4) | | | | |
| | | S(3)−O(2) | 1.483(4) | | | | |
| | | S(3)−O(6) | 1.483(4) | | | | |
| | | S(3)−O(5) | 1.496(4) | | | | |

performance focusing Quazar multilayer optics. Standard SAINT software was used for determination of the unit cells and data collection control. The intensities of reflections of a sphere were collected by a combination of multiple sets of exposures (frames). Each set had a different $\varphi$ angle for the crystal, and each exposure covered a range of 0.5° in $\omega$. A total of 1464 frames were collected with exposure times of 10−40 s depending on the crystal. The SAINT software was used for data integration including Lorentz and polarization corrections. Crystals of $RbU(SO_4)_2$, $CsU(SO_4)_2$, and $KNp(SO_4)_2$ were nonmerohedrally twinned with a rotation angle of 180°. Crystals of $KNp(SO_4)_2(H_2O)$ contained disordered K and Np atom positions and were refined accordingly. The program CELL_NOW was used to index the twin crystals where necessary. Multi-Scan absorption corrections were applied using the program SADABS or TWINABS.[59−61] The structure was solved by direct methods and refined on $F^2$ by full-matrix least-squares techniques using the program suite SHELX.[62] Solutions were checked using PLATON.[63]

**UV−vis−NIR Spectroscopy.** Ultraviolet−visible−near-infrared (UV−vis−NIR) data were acquired from single or twinned crystals using a Craic Technologies microspectrophotometer. Crystals were placed on quartz slides under Krytox oil, and the data were collected from 200 to 1500 nm with only the area of interest shown in Figures.

**Magnetic Measurements.** Magnetic measurements were performed on polycrystalline samples with a Quantum Design SQUID magnetometer MPMS-XL. Direct current magnetic susceptibility measurements were carried out in an applied field of 0.100 T in the 1.8−300 K temperature range. Field-dependent magnetization was recorded at 1.8 K with the magnetic field varying from 0 to 7 T.

## RESULTS AND DISCUSSION

**Synthesis.** The syntheses of all products were accomplished utilizing Zn amalgam as an *in situ* reductant and by taking no regard to the presence of oxygen. This is in stark contrast to the


dx.doi.org/10.1021/ic500771t | Inorg. Chem. 2014, 53, 7455−7466

**Table 3. Crystallographic Information for Np Compounds**

| compound | $NaNp(SO_4)_2(H_2O)$ | $KNp(SO_4)_2(H_2O)$ | $KNp(SO_4)_2$ | $RbNp(SO_4)_2$ | $CsNp(SO_4)_2$ |
|---|---|---|---|---|---|
| formula mass | 470.11 | 486.22 | 468.22 | 514.59 | 562.03 |
| color and habit | purple-blue, prism | purple-blue, prism | purple; block | purple-blue, plate | purple-blue, plate |
| space group | $P3_12_1$ | $P3_12_1$ | $P\bar{1}$ | $P2_1/n$ | $P2_1/n$ |
| $a$ (Å) | 7.0147(6) | 7.196(1) | 5.411 (2) | 9.127(4) | 5.448(1) |
| $b$ (Å) | 7.0147(6) | 7.196(1) | 6.949(2) | 5.414(2) | 14.333(3) |
| $c$ (Å) | 12.909(1) | 13.386(4) | 8.378(3) | 14.198(5) | 9.400(2) |
| $a$ (deg) | 90 | 90 | 86.445(3) | 90 | 90 |
| $\beta$ (deg) | 90 | 90 | 88.413(3) | 102.715(5) | 90.344(2) |
| $\gamma$ (deg) | 120 | 120 | 88.552(3) | 90 | 90 |
| $V$ (Å$^3$) | 550.12(8) | 600.3(2) | 314.2(2) | 684.4(5) | 734.0(2) |
| $Z$ | 3 | 3 | 2 | 4 | 4 |
| $T$ (K) | 296 | 296 | 100 | 296 | 296 |
| $\lambda$ (Å) | 0.710 73 | 0.710 73 | 0.710 73 | 0.710 73 | 0.710 73 |
| maximum $2\Theta$ (deg) | 27.52 | 27.19 | 26.74 | 27.56 | 27.60 |
| $\rho_{calcd}$(g·cm$^{-3}$) | 4.239 | 4.018 | 4.948 | 4.994 | 5.086 |
| $\mu$(Mo K$\alpha$) (cm$^{-1}$) | 148.18 | 140.45 | 178.68 | 228.66 | 196.20 |
| $R(F)$ for $F_0^2 > 2s(F_0^2)^a$ | 0.0194 | 0.0312 | 0.0325 | 0.0253 | 0.0278 |
| $R_w(F_0^2)^b$ | 0.0528 | 0.0715 | 0.0813 | 0.0574 | 0.0738 |

$^aR(F) = \Sigma||F_0| - |F_c||/\Sigma|F_0|$. $^bR_w(F_0^2) = [\Sigma[w(F_0^2 - F_c^2)^2]/\Sigma wF_0^4]^{1/2}$.

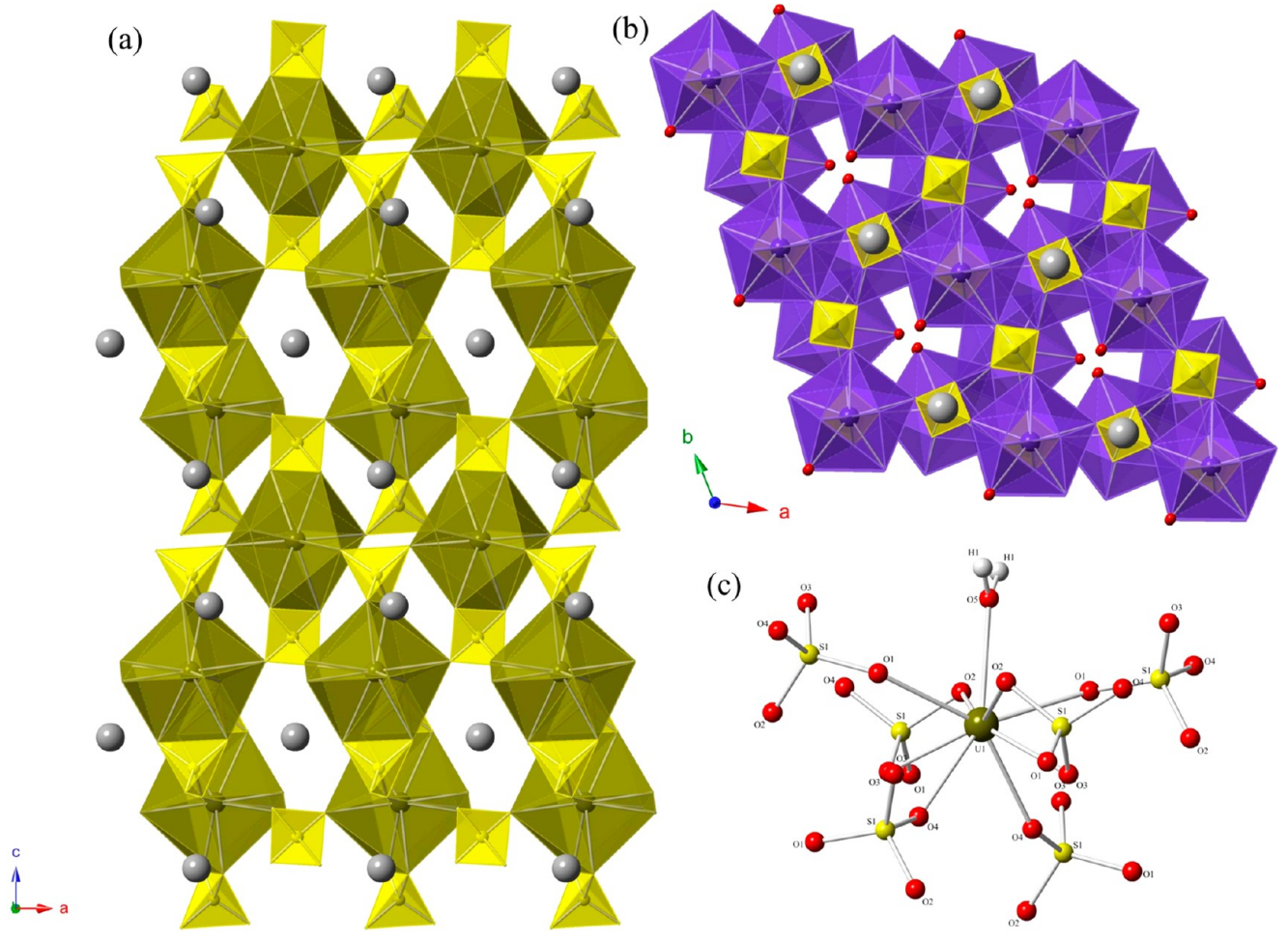


**Figure 1.** Structural views of $AAn(SO_4)_2(H_2O)$ (A = Na, K) (An = $U^{3+}$, $Np^{3+}$). (a) The polyhedral view of $NaU(SO_4)_2(H_2O)$ along the $b$ axis, where gray spheres are Na, yellow tetrahedra are $SO_4^{2-}$ anions, and olive polyhedra are $U^{3+}$ metal centers. (b) The same structure type but with the purple polyhedra representing $Np^{3+}$ along the $c$ axis with a clear view of the 3-fold rotation red spheres that are representative of the coordinating water. (c) The ball-and-stick representation of the $U^{3+}$ coordination where the U atom is an olive sphere, O atoms are red spheres, S atoms are yellow spheres, and H atoms are white spheres.


dx.doi.org/10.1021/ic500771t | Inorg. Chem. 2014, 53, 7455−7466

**Table 4. Selected Bond Distances for Np Compounds**

| $NaNp(SO_4)_2(H_2O)$ | | $KNp(SO_4)_2(H_2O)$ | | $KNp(SO_4)_2$ | | $RbU(SO_4)_2$ | | $CsU(SO_4)_2$ | |
|---|---|---|---|---|---|---|---|---|---|
| Np(1)−O(3) | 2.474(5) | Np(1)−O(1) | 2.514(9) | Np(1)−O(7) | 2.434(7) | Np(1)−O(7) | 2.442(5) | Np(1)−O(6) | 2.467(6) |
| Np(1)−O(3)′ | 2.474(5) | Np(1)−O(1) | 2.514(9) | Np(1)−O(8) | 2.489(7) | Np(1)−O(1) | 2.480(4) | Np(1)−O(3) | 2.479(6) |
| Np(1)−O(4) | 2.494(5) | Np(1)−O(5) | 2.63(3) | Np(1)−O(1) | 2.491(7) | Np(1)−O(3) | 2.481(4) | Np(1)−O(2) | 2.487(6) |
| Np(1)−O(4)′ | 2.494(5) | Np(1)−O(2) | 2.70(1) | Np(1)−O(4) | 2.520(6) | Np(1)−O(6) | 2.505(5) | Np(1)−O(1) | 2.496(7) |
| Np(1)−O(1W) | 2.54(1) | Np(1)−O(2)′ | 2.70(1) | Np(1)−O(2) | 2.533(6) | Np(1)−O(8) | 2.506(5) | Np(1)−O(4) | 2.499(7) |
| Np(1)−O(1) | 2.567(4) | Np(1)−O(3) | 2.73(1) | Np(1)−O(6) | 2.557(7) | Np(1)−O(2) | 2.534(5) | Np(1)−O(5) | 2.551(7) |
| Np(1)−O(1)′ | 2.567(4) | Np(1)−O(3)′ | 2.73(1) | Np(1)−O(5) | 2.590(6) | Np(1)−O(5) | 2.566(5) | Np(1)−O(7) | 2.570(9) |
| Np(1)−O(2) | 2.572(4) | Np(1)−O(4) | 2.76(1) | Np(1)−O(3) | 2.596(7) | Np(1)−O(4) | 2.736(5) | Np(1)−O(8) | 2.729(9) |
| Np(1)−O(2) | 2.573(4) | Np(1)−O(4)′ | 2.76(1) | Np(1)−O(6) | 2.810(6) | Np(1)−O(4) | 2.748(5) | S(1)−O(6) | 1.457(7) |
| S(1)−O(1) | 1.464(5) | Np(2)−O(2) | 2.52(1) | S(1)−O(8) | 1.455(7) | S(1)−O(8) | 1.465(5) | S(1)−O(3) | 1.467(6) |
| S(1)−O(3) | 1.464(5) | Np(2)−O(2)′ | 2.52(1) | S(1)−O(2) | 1.476(6) | S(1)−O(6) | 1.473(5) | S(1)−O(5) | 1.476(7) |
| S(1)−O(4) | 1.471(4) | Np(2)−O(5) | 2.59(2) | S(1)−O(5) | 1.486(7) | S(1)−O(3) | 1.481(5) | S(1)−O(7) | 1.485(7) |
| S(1)−O(2) | 1.481(4) | Np(2)−O(1) | 2.67(1) | S(1)−O(1) | 1.492(6) | S(1)−O(4) | 1.501(5) | S(2)−O(1) | 1.457(7) |
| | | Np(2)−O(1)′ | 2.67(1) | S(2)−O(3) | 1.458(7) | S(2)−O(1) | 1.473(5) | S(2)−O(4) | 1.468(6) |
| | | Np(2)−O(3) | 2.70(1) | S(2)−O(4) | 1.472(7) | S(2)−O(7) | 1.477(5) | S(2)−O(2) | 1.476(6) |
| | | Np(2)−O(3)′ | 2.70(1) | S(2)−O(7) | 1.480(7) | S(2)−O(5) | 1.482(5) | S(2)−O(8) | 1.479(7) |
| | | Np(2)−O(4) | 2.70(1) | S(2)−O(6) | 1.495(7) | S(2)−O(2) | 1.483(5) | | |
| | | Np(2)−O(4)′ | 2.70(1) | | | | | | |
| | | S(1)−O(4) | 1.45(1) | | | | | | |
| | | S(1)−O(3) | 1.459(9) | | | | | | |
| | | S(1)−O(2) | 1.48(1) | | | | | | |
| | | S(1)−O(1) | 1.485(9) | | | | | | |

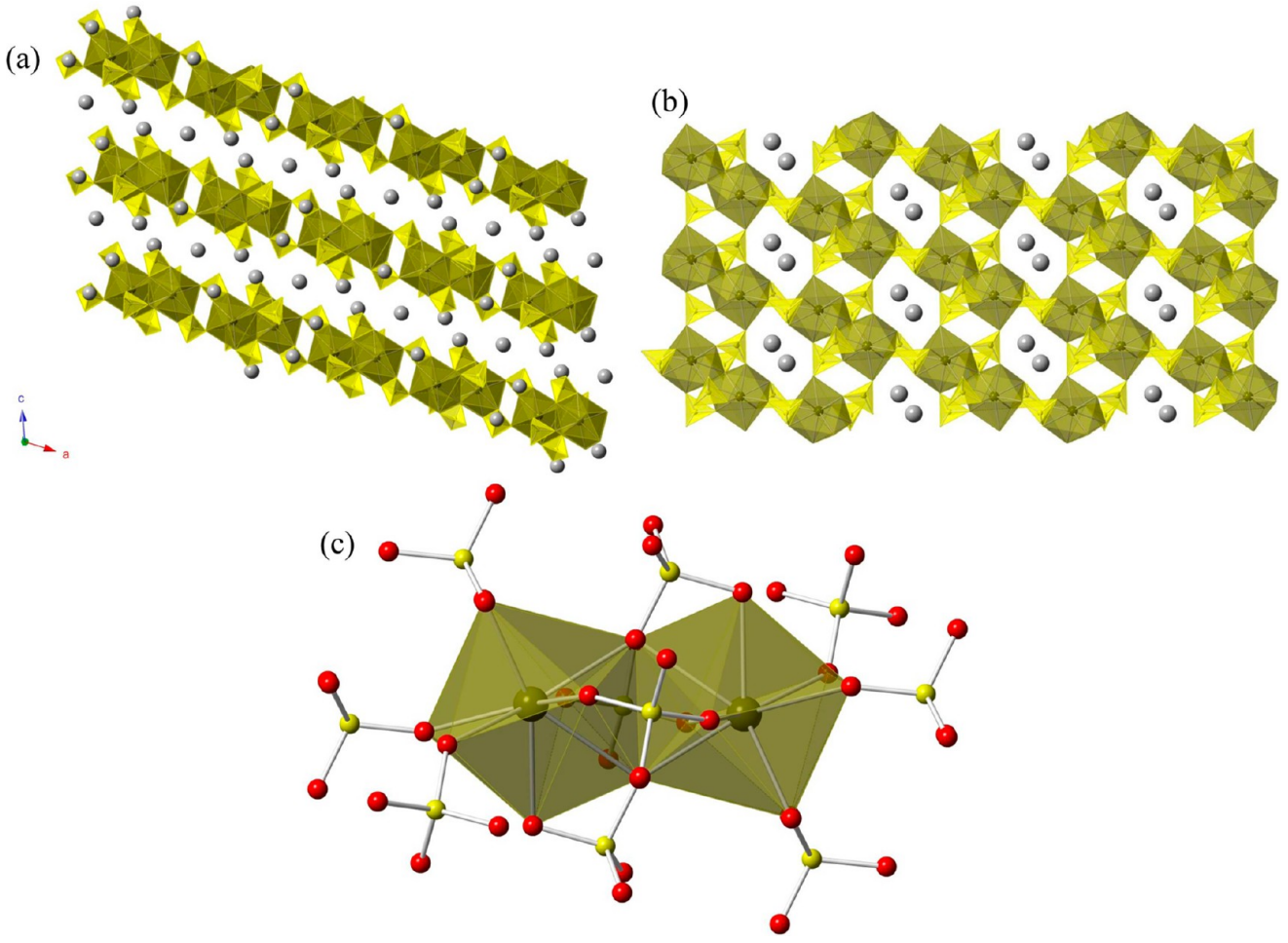


**Figure 2.** Structural views of the mixed-valent $K_5U_2(SO_4)_6H_2O$. (a) The polyhedral view of $K_5U_2(SO_4)_6H_2O$ along the *b* axis where gray spheres are K, yellow tetrahedral are $SO_4^{2-}$ anions, and olive polyhedra are $U^{3+}$ metal centers. (b) An isolated layer where the U dimers can be seen. (c) The $U^{3+}$ coordination edge-sharing dimer where the U polyhedra are olive, O atoms are red spheres, and S atoms are yellow spheres.


dx.doi.org/10.1021/ic500771t | *Inorg. Chem.* 2014, 53, 7455−7466

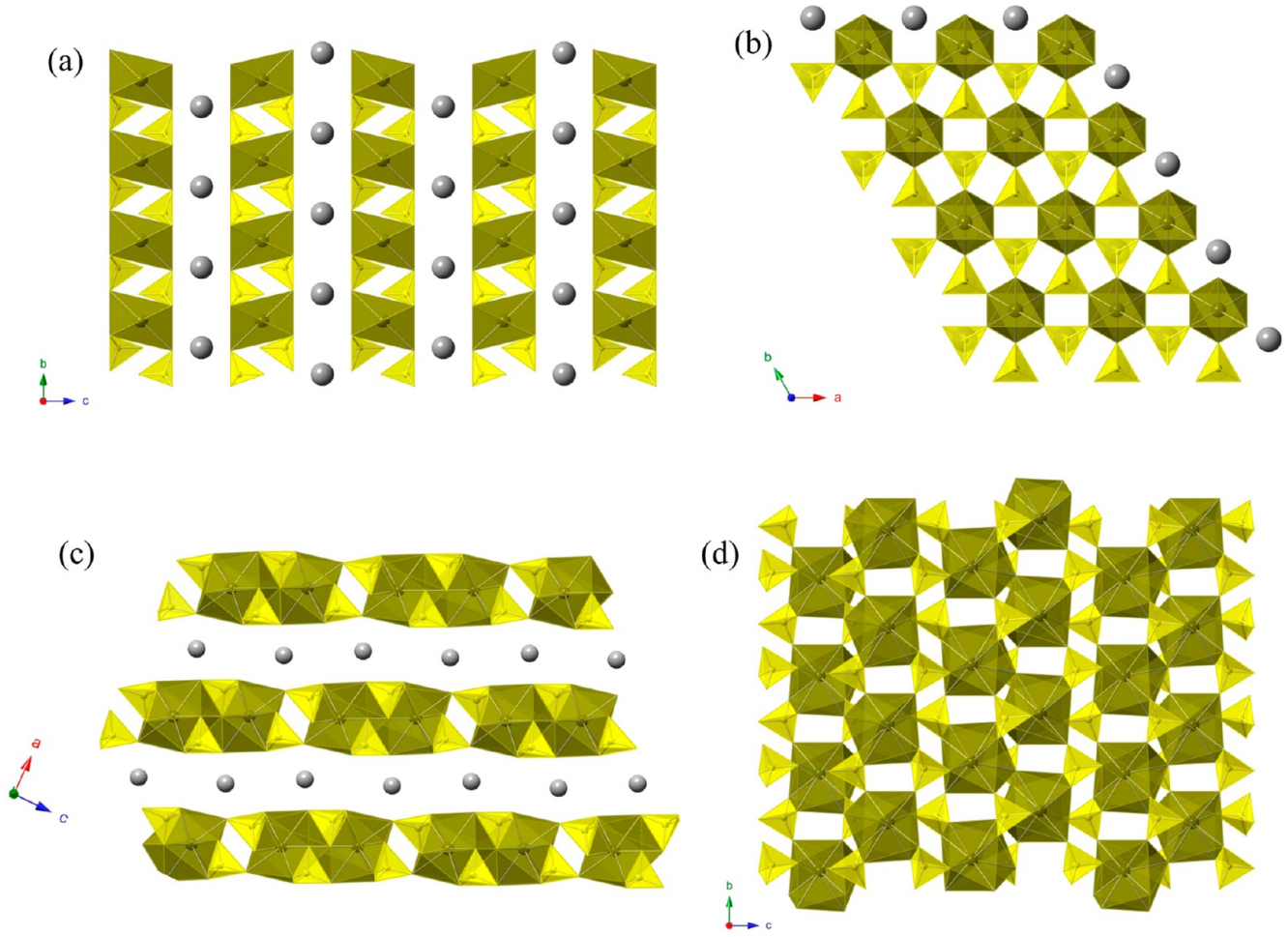


**Figure 3.** Structural views of $RbU(SO_4)_2$ [(a) and (b)] and $CsU(SO_4)_2$ [(c) and (d)]. (a) The polyhedral view of the layered structure $RbU(SO_4)_2$ along the *a* axis where gray spheres are Rb, yellow tetrahedral are $SO_4^{2-}$ anions, and olive polyhedra are $U^{3+}$ metal centers. (b) An isolated layer where the distorted U octahedra can clearly be seen. (c) The polyhedral view of the similarly layered structure $CsU(SO_4)_2$ along the *b* axis where gray spheres are Cs, yellow tetrahedral are $SO_4^{2-}$ anions, and olive polyhedra are $U^{3+}$ metal centers. (d) shows an isolated layer where the distorted U tricapped trigonal prisms corner share.

conventional methods where trivalent products cannot be obtained unless oxygen is excluded. Careful control of the pH to 0 is necessary to facilitate these reactions as reduction becomes increasingly difficult as pH increases. Green crystals of $U^{4+}$ byproduct were obtained in all reactions where $U^{3+}$ was obtained with the exception of the $Na_2CO_3$ reaction where only $NaU(SO_4)_2(H_2O)$ was isolated. The amount of $U^{3+}$ product increased with increasing time to 12 h. Beyond that time, more $U^{4+}$ product was obtained. Np reactions were carried out on a much smaller scale than the U reactions, and although the molarity of reagents is changed the mole ratio was kept the same as in the U reactions. The reactivity of Np diverges from U in that only $Np^{3+}$ products were obtained, and the only reaction yielding an isotypic product was the $Na_2CO_3$ reaction. The presence of only $Np^{3+}$ makes sense when the reduction potentials are taken into account as the $U^{4+}$ to $U^{3+}$ reduction potential is −0.607 V making it difficult to overcome whereas the $Np^{4+}$ to $Np^{3+}$ potential is only 0.147 V, making it a much more feasible reduction. Zn amalgam has a reduction potential of 0.762 V, which is above what is needed to reduce both U and Np to the trivalent state especially when present in large excess. After each reaction the Zn amalgam is washed with water and reused for subsequent reactions until most of the Zn is oxidized and the disc no longer holds shape. All of the products obtained are air and water stable: crystals were left unchanged after repeated washings and did not show observable changes in crystallinity or color when stored under ambient conditions.

**Structure and Topological Description.** *$AEAn(SO_4)_2(H_2O)$ (AE = Na, K) (An = U, Np).* The compounds $NaU(SO_4)_2(H_2O)$, $NaNp(SO_4)_2(H_2O)$, and $KNp(SO_4)_2(H_2O)$ are all isotypic and crystallize in the chiral space group $P3_12_1$ or its enantiomer $P3_22_1$ (crystallographic data in Tables 1 and 3). This structure type is a dense three-dimensional (3D) framework whose main features are trigonal helixes. The 3D framework is formed by alternating $AE^+$ and $An^{3+}$ cations forming corrugated layers, which are linked by the sulfate anion that edge shares with one An polyhedron and then corner shares to two other An polyhedra. The alternating cations allow for the disorder of AE and An atoms seen in the $KNp(SO_4)_2(H_2O)$ structure. The analogous lanthanide structures for $NaAn(SO_4)_2(H_2O)$ have been synthesized with La−Gd.[64−67] Only one example of this structure type has been reported with K, namely, $KLa(SO_4)_2(H_2O)$.[68] The An center is a nine-coordinate tricapped trigonal prism where eight O atoms are donated from sulfate groups and the apical O atom is a coordinating water. Views along the *a* and *c* axis along with the coordination geometry of the An center are shown in Figure 1. The average U−O bond distance is 2.54(4) Å, which sits in between typical La−O and Ce−O bond lengths,


dx.doi.org/10.1021/ic500771t | *Inorg. Chem.* 2014, 53, 7455−7466

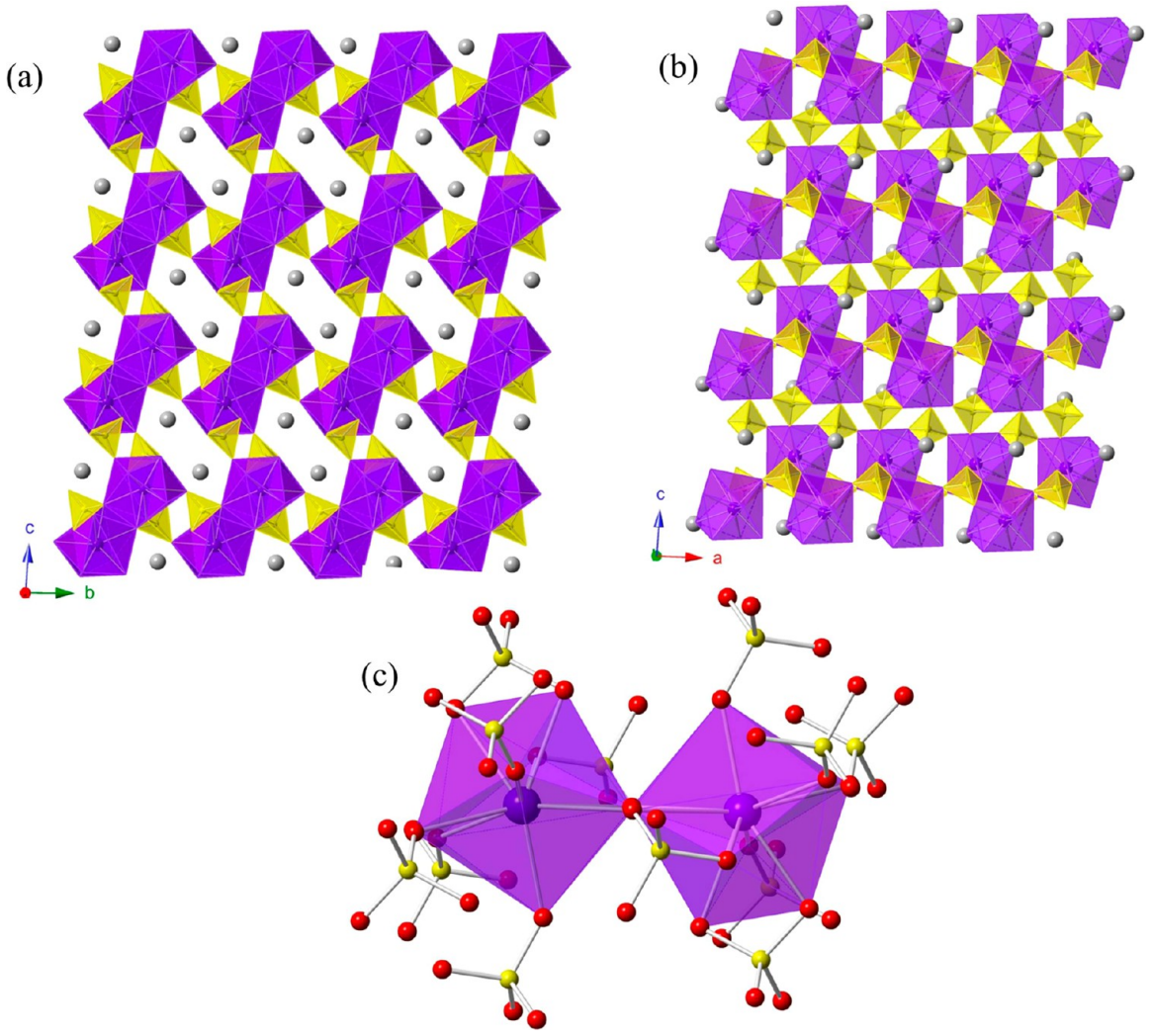


**Figure 4.** Structural views of the anhydrous $KNp(SO_4)_2$. (a) The polyhedral view of $KNp(SO_4)_2$ along the *a* axis where gray spheres are K, yellow tetrahedral are $SO_4^{2-}$ anions, and purple polyhedra are $Np^{3+}$ metal centers. (b) The view along the *b* axis. (c) The $Np^{3+}$ coordination edge-sharing dimer where the Np polyhedra are purple, O atoms are red spheres, and S atoms are yellow spheres.

which are 2.55(4) Å and 2.53(3) Å, respectively. The average Np−O distance is the same as the typical Ce−O distance at 2.53(4) Å (see selected bond distances in Tables 2 and 4). Because of the disorder between the K and Np atoms in $KNp(SO_4)_2(H_2O)$ no reasonable comparisons can be made between the bond distances in the structures.

*$K_5U_2(SO_4)_6(H_2O)$.* $K_5U_2(SO_4)_6H_2O$ crystallizes in the space-group *C*2/*c* and has a sheet topology that features U polyhedra as edge-sharing dimers connected by sulfate groups with K and $H_2O$ in the interlayer space. The formula only charge balances when U is considered to be half $U^{3+}$ and half $U^{4+}$. This finding coincides with the assessment made for the Ce analogue of this compound and is reflected in the absorption spectra shown in Figure 2.[69,70] The U polyhedron is a nine-coordinate tricapped trigonal prism with an average U−O bond distance of 2.48(4) Å, which is about the same as the Ce−O average bond length (2.47(7) Å). All of the O atoms are donated from sulfate groups. The charge distribution of $U^{3+}$ and $U^{4+}$ is considered spread over the two U sites and is not resolved even when moving to the lower-symmetry space group *Cc*, which crystallographically separates the dimer. The S1 sulfate anion is edge-sharing with one U polyhedron while one of the edge-sharing O atoms is corner-sharing with another U polyhedra making it a $\mu$-3 O atom. The S2 group corner shares between three U polyhedra. The S3 group edge shares with one U polyhedron and corner shares with another U polyhedron forming the layers as shown in Figure 2.

*$RbU(SO_4)_2$.* $RbU(SO_4)_2$ is the only $U^{3+}$ compound that does not have a lanthanide analogue. $RbU(SO_4)_2$ crystallizes in the space group $P6_3/mmc$ and is a sheet structure with distorted $UO_6$ octahedra and sulfate groups separated by Rb atoms. All O atoms in the U octahedra are donated from sulfate groups and have equal 2.50(1) Å U−O bond lengths. Each sulfate group corner shares three O atoms with three different ocatahedra, forming sheets in the *ab* plane as shown in Figure 3.

*$CsU(SO_4)_2$.* $CsU(SO_4)_2$ crystallizes in the space group $P2_1/n$ and is also a sheet-type topology where Cs atoms separate layers of sulfate tetrahedra and U polyhedra. The U polyhedra are nine-coordinate tricapped trigonal prisms where all O atoms are donated from sulfate groups. The average U−O bond length is 2.57(4) Å, which is smaller than the average La−O distance of the isotypic structure at 2.59(5) Å.[71] The S1 group edge shares with one U polyhedron while corner sharing two different polyhedra. The S2 group edge shares with two different U polyhedra, forming a corner sharing interaction between them, and corner shares to a third U polyhedron as shown in Figure 3.


dx.doi.org/10.1021/ic500771t | *Inorg. Chem.* 2014, 53, 7455−7466

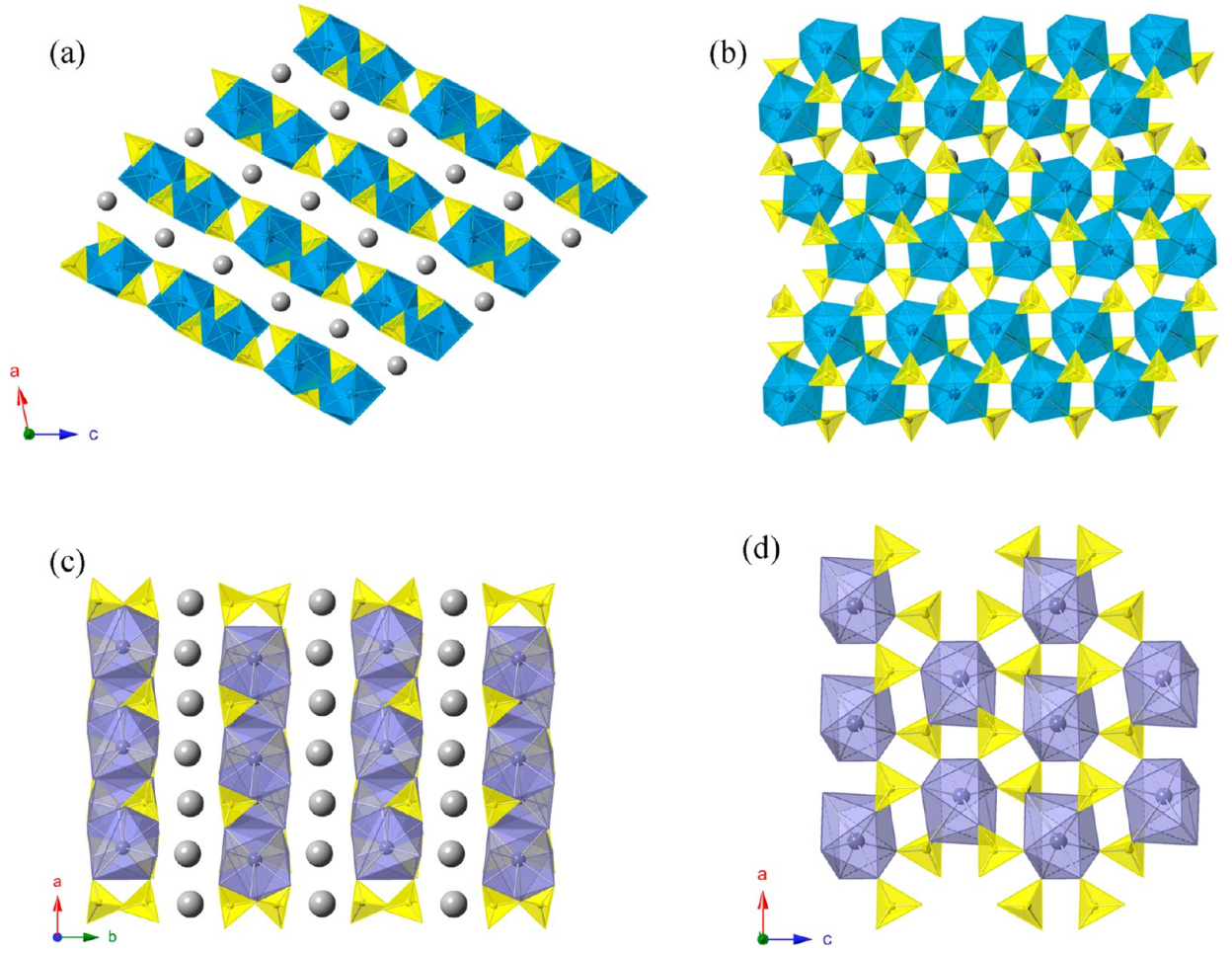


**Figure 5.** Structural views of $RbNp(SO_4)_2$ [(a) and (b)] and $CsNp(SO_4)_2$ [(c) and (d)]. (a) The polyhedral view of the layered structure $RbU(SO_4)_2$ along the *a* axis where gray spheres are Rb, yellow tetrahedral are $SO_4^{2-}$ anions, and blue polyhedra are $Np^{3+}$ metal centers. (b) An isolated layer where the distorted Np monocapped square antiprisms corner share. (c) The polyhedral view of the similarly layered structure $CsNp(SO_4)_2$ along the *b* axis where gray spheres are Cs, yellow tetrahedral are $SO_4^{2-}$ anions, and light-purple polyhedra are $Np^{3+}$ metal centers. (d) A layer along the *b* axis where the distorted Np square antiprisms are isolated from each other.

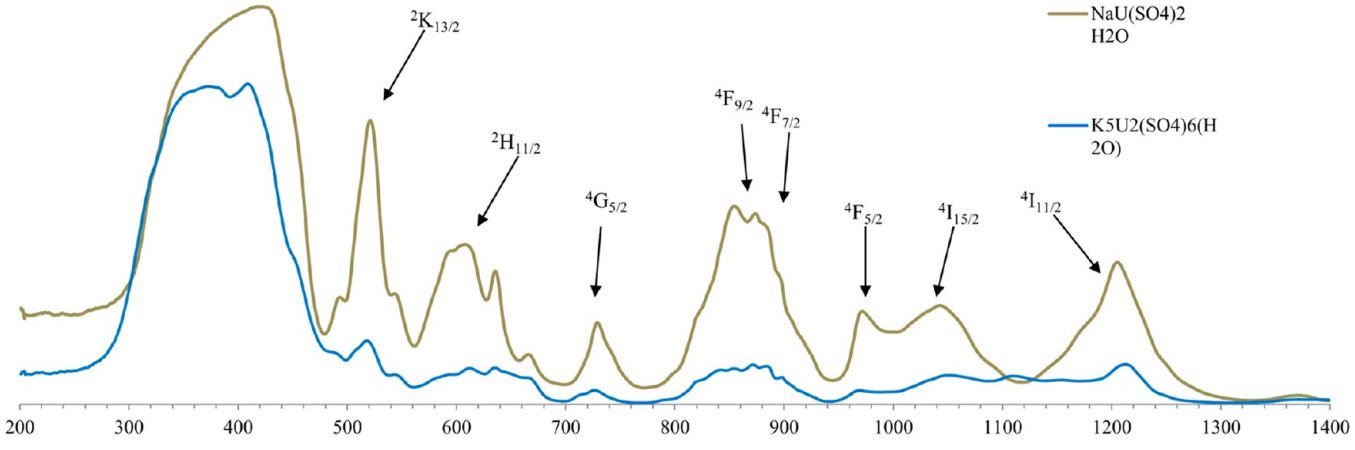


**Figure 6.** Solid-state absorption spectra of $NaU(SO_4)_2(H_2O)$ (olive) and the mixed-valent $K_5U_2(SO_4)_6H_2O$ (blue). The $NaU(SO_4)_2(H_2O)$ is a typical $U^{3+}$ spectra with the signature transitions being the $^4G_{5/2}$ at 730 nm and the $^4I_{11/2}$ transition at 1200 nm. The large peak from approximately 300 to 450 nm is the parity-allowed f −d transition. Other significant peaks are labeled. The $K_5U_2(SO_4)_6H_2O$ has much weaker absorbance, but the $U^{3+}$ and $U^{4+}$ transitions are still visible. The absorbance at 1100 nm distinguishes the tetravalent character.

*$KNp(SO_4)_2$.* $KNp(SO_4)_2$ is the secondary, anhydrous product obtained along with $KNp(SO_4)_2H_2O$. It crystallizes in the space group $P\bar{1}$ and is a 3D framework. The Np polyhedra are nine-coordinate distorted tricapped trigonal prisms where all O atoms are donated from sulfate anions. The Np polyhedra form edge-sharing dimers that are linked by sulfate. Both sulfate groups edge share with one Np center and corner share with two other Np centers forming channels down the *a* axis where the $K^+$ cations sit


dx.doi.org/10.1021/ic500771t | *Inorg. Chem.* 2014, 53, 7455−7466

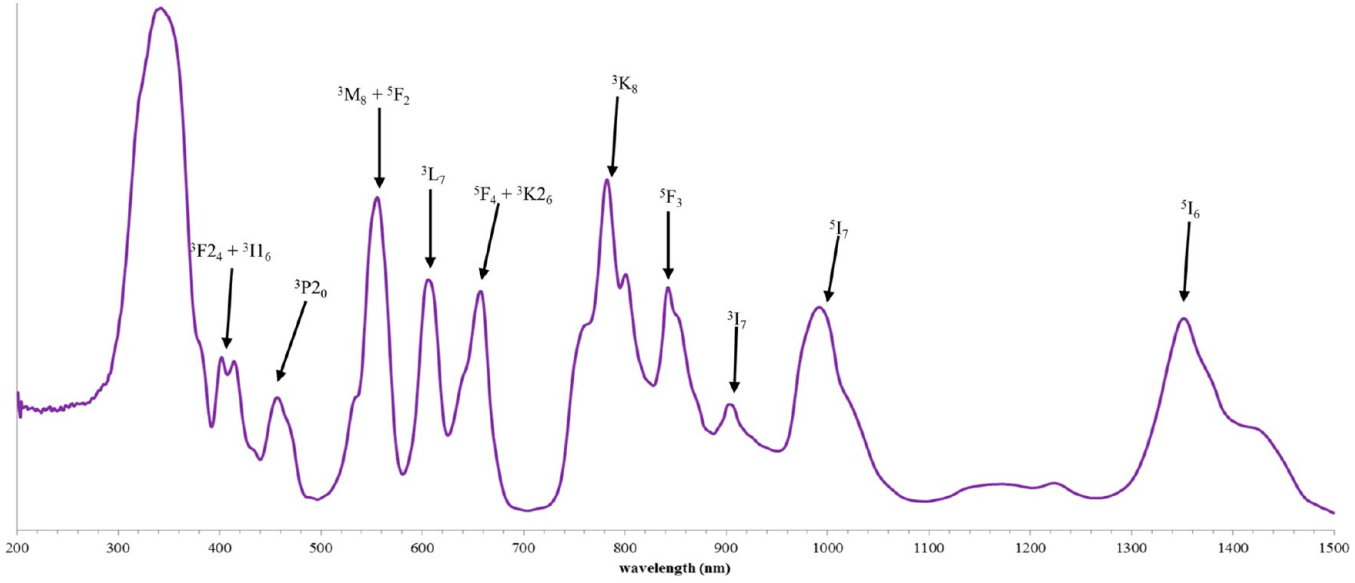


**Figure 7.** Solid-state absorption spectrum of $NaNp(SO_4)_2(H_2O)$ (purple) with labeled transitions. The signature transitions of $NaNp(SO_4)_2(H_2O)$ are the three peaks centered around 600 nm and the $^5I_6$ transition at 1350 nm. The peak from approximately 300 to 390 nm is the parity-allowed f −d transition, which is much smaller than the $U^{3+}$ f-d peak.

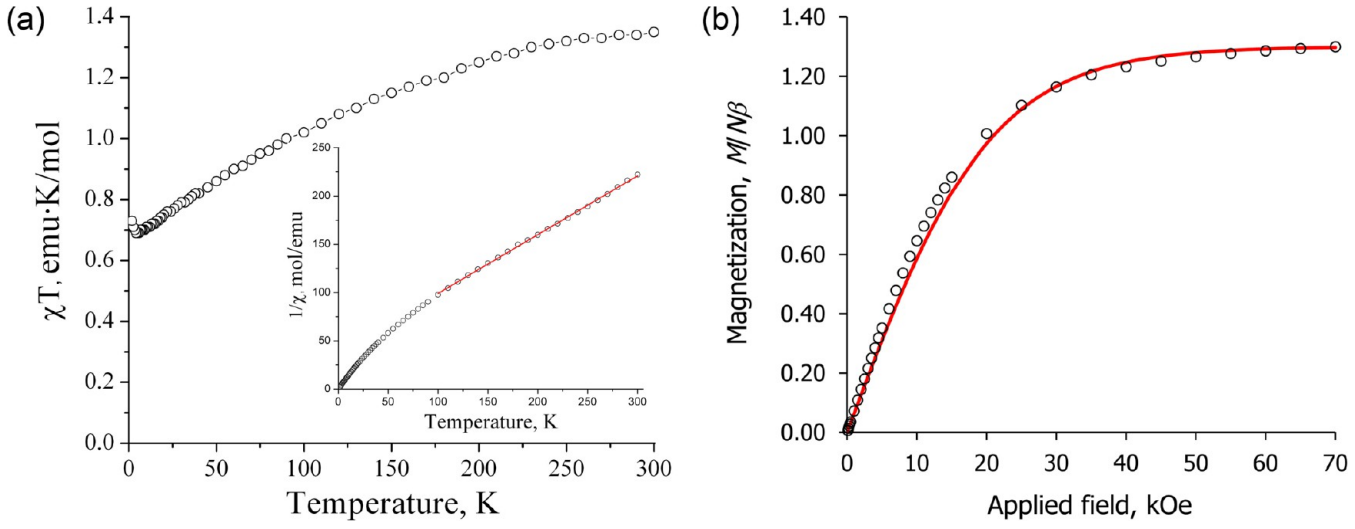


**Figure 8.** Magnetic properties of $NaU(SO_4)_2(H_2O)$. (a) Temperature dependence of $\chi T$. (inset) the Curie−Weiss fit (solid red line) for the $1/\chi$ vs $T$ dependence in the high-temperature region. (b) Field dependence of magnetization per U atom at 1.8 K; red line shows the fit to the Brillouin function for $S = 1/2$, $g = 2.6$.

as shown in Figure 4. The Np−O bond distances range from 2.434(7) to 2.810(6) Å. This structure type has been previously reported for Pr where it was synthesized at higher temperatures.[72]

*RbNp(SO4)2*. $RbNp(SO_4)_2$ crystallizes in the space group $P2_1/n$ and is a sheet-type topology where Rb atoms separate layers of sulfate tetrahedra and Np polyhedra. Again, the Rb congener has no lanthanide analogue. The Np polyhedra are nine-coordinate distorted monocapped square antiprisms where all O atoms are donated from sulfate groups. The Np−O distances range from 2.442(5) to 2.748(5) Å. The S1 group is edge-sharing with one Np polyhedron while one of the edge-sharing O atoms is corner-sharing with another Np polyhedron making it a $\mu$-3 O atom. The corner-sharing Np polyhedra form zigzag chains along the $b$ axis. The S2 group edge shares with one Np polyhedron and corner shares the remaining two O atoms to two separate Np polyhedra forming the overall layer topology.

*CsNp(SO4)2*. $CsNp(SO_4)_2$ crystallizes in the space group $P2_1/n$ and has a sheet-type topology where Cs atoms separate the layers of sulfate tetrahedra and Np polyhedra similar to those of $RbNp(SO_4)_2$. The Np polyhedra are eight-coordinate square antiprisms with approximate $D_{4d}$ symmetry where all O atoms are donated from sulfate anions.[73,74] The average Np−O bond distance is 2.53(8) Å. Both sulfate groups edge share with one Np center and corner share with two other Np centers. There is no sharing of any kind between the Np polyhedra. This structure type has been previously reported for $CsPr(SO_4)_2$.[75] Polyhedral representations of $RbNp(SO_4)_2$ and $CsNp(SO_4)_2$ are shown in Figure 5.

*UV−vis−NIR Absorption Spectroscopy*. The single-crystal UV−vis−NIR absorption spectra of the $NaU(SO_4)_2(H_2O)$ and


dx.doi.org/10.1021/ic500771t | Inorg. Chem. 2014, 53, 7455−7466

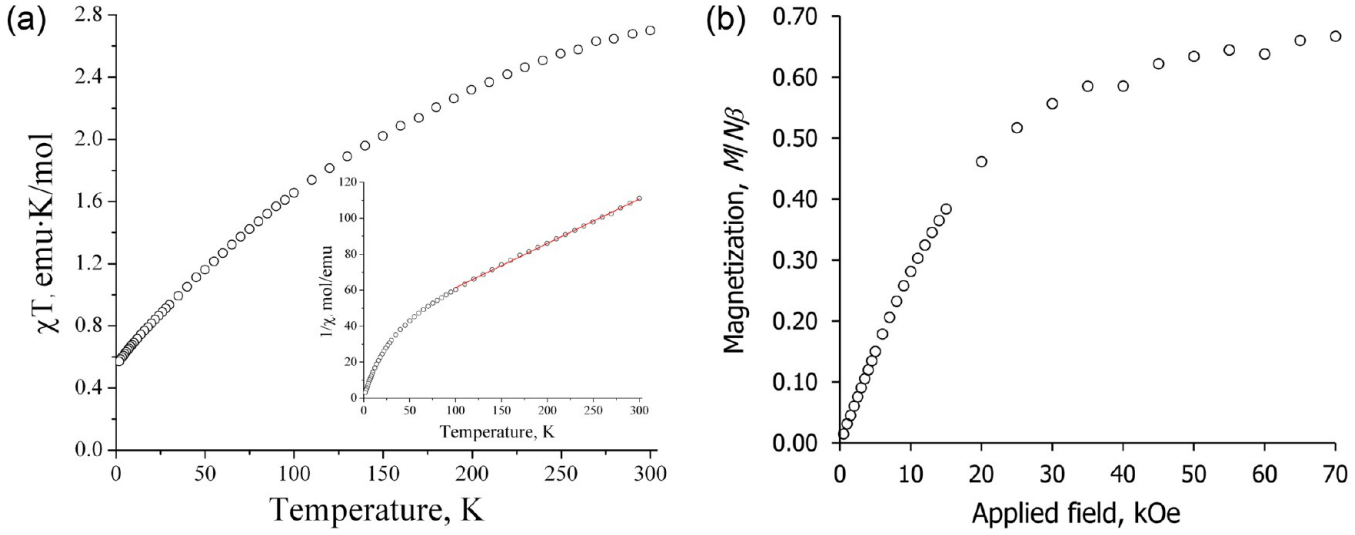


**Figure 9.** Magnetic properties of $K_5U_2(SO_4)_6(H_2O)$. (a) Temperature dependence of $\chi T$. (inset) The Curie–Weiss fit (solid red line) for the $1/\chi$ vs $T$ dependence in the high-temperature region. (b) Field dependence of magnetization per U atom at 1.8 K.

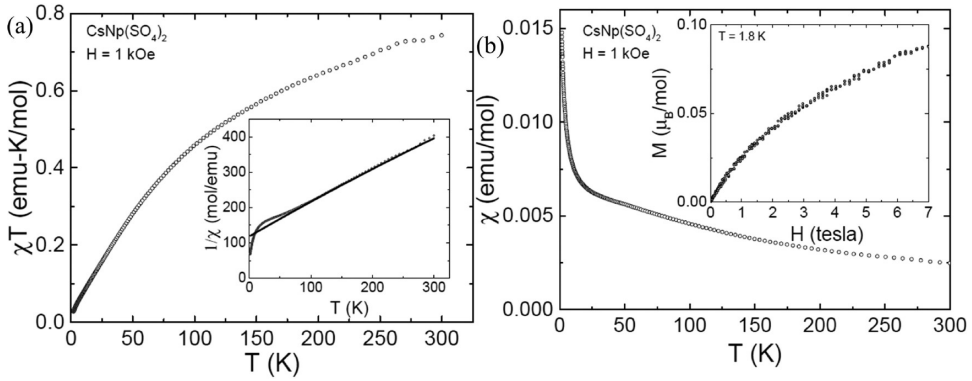


**Figure 10.** Magnetic susceptibility for $CsNp(SO_4)_2$ as a function of $T$ and $H$. (a) $\chi T$ vs $T$ and $\chi^{-1}$ vs $T$ (inset). (b) $\chi$ vs $T$ and magnetization vs magnetic field (inset).

$K_5U_2(SO_4)_6(H_2O)$ compounds are shown in Figure 6. The transitions of $U^{3+}$ have been thoroughly characterized.[36,76,77] The strongest absorption in all the spectra is the f–d transition from approximately 300 to 450 nm. The first f–f peak is at approximately 450 nm, which is the transition from the $^4I_{9/2}$ ground state of $U^{3+}$ to the $^2G_{7/2}$ excited state. The signature peaks of $U^{3+}$ are the 520 nm $^2K_{13/2}$, the 750 nm $^4G_{5/2}$, and the 1210 nm $^4I_{11/2}$ transitions. These are in close agreement with previously reported $U^{3+}$ spectra.[29,34] The $K_5U_2(SO_4)_6(H_2O)$ spectra is somewhat different than the other spectra. This is attributed to the mixed valency of U and can be understood as a combination of the $U^{3+}$ and $U^{4+}$ spectra. This can easily be seen in the NIR region where $U^{3+}$ has a series of peaks from 950 to 1050 nm, which then drops off around 1100 nm. This drop-off is not seen in the spectra of $K_5U_2(SO_4)_6H_2O$ because $U^{4+}$ has a significant peak at 1100 nm.

The labeled single-crystal UV–vis–NIR absorption spectrum of $NaNp(SO_4)_2(H_2O)$ is shown in Figure 7 with additional spectra shown in Supporting Information, Figures S15–S17. The spectrum is in good agreement with previously reported $Np^{3+}$ spectra.[36,38,76,78,79] Analysis of the electronic transitions has been reported previously as well. $Np^{3+}$ possesses a $^5I_4$ ground-state configuration. There are many peaks in the $Np^{3+}$ spectra that overlap with the $Np^{4+}$ spectra, but a characteristic $Np^{3+}$ peak can be found at 1360 nm, which is the $^5I_6$ transition. Other important transitions can be found in Figure 7.

**Magnetism.** *$NaU(SO_4)_2(H_2O)$.* For this compound, the $\chi T$ product exhibits strong temperature dependence indicating significant deviation from the Curie behavior (Figure 8a). Fitting the linear part of the temperature dependence of inverse magnetic susceptibility to the Curie–Weiss law (Figure 8a, inset) gave a negative value of the Weiss constant, $\theta = -63(2)$ K, but no signature of magnetic ordering was observed. Given the significant separation between the $U^{3+}$ ions in the crystal structure of the compound, with the nearest U–U distance being 5.61 Å, the appreciable value of $\theta$ likely indicates the depopulation of higher excited states rather than antiferromagnetic coupling of such magnitude. The Curie constant was found to be 1.64(1) emu·mol$^{-1}$·K per formula unit, which results in the effective magnetic moment of 3.62 $\mu_B$ per U atom. This value is comparable to those found in the literature.[30] The field-dependent magnetization measured at 1.8 K approaches saturation at 7 T (Figure 8b). A satisfactory fit was obtained using the Brillouin function for $J = 1/2$, which suggests stabilization of an effective ground-state doublet with $g_{eff} = 2.60(2)$ due to the crystal-field splitting and depopulation of the excited states at low temperatures.

*$K_5U_2(SO_4)_6(H_2O)$.* Similar to the Na-containing compound, no magnetic ordering was detected for $K_5U_2(SO_4)_6(H_2O)$. The $\chi T$


dx.doi.org/10.1021/ic500771t | Inorg. Chem. 2014, 53, 7455–7466

product also exhibits strong temperature dependence, and in this case the deviation from the Curie behavior is even stronger (Figure 9a). Fitting the linear part of the temperature dependence of inverse magnetic susceptibility to the Curie–Weiss law (Figure 9a, inset) gave a negative value of the Weiss constant, $\theta = -148(2)$ K. A comparison to $NaU(SO_4)_2(H_2O)$ suggests that more significant magnetic exchange coupling might be operating in $K_5U_2(SO_4)_6(H_2O)$, which could be expected from the mixed valence of U in this compound. The Curie constant is 4.05(3) emu·mol$^{-1}$·K per formula unit, which results in the effective magnetic moment of 4.02 $\mu_B$ per U atom. The field-dependent magnetization measured at 1.8 K is relatively low, attaining the value of only 0.67 $\mu_B$ per U atom at the maximum applied field of 7 T (Figure 9b). The suppressed magnetization values as compared to those observed for $NaU(SO_4)_2(H_2O)$ also support stronger antiferromagnetic short-range correlations in $K_5U_2(SO_4)_6(H_2O)$.

*$CsNp(SO_4)_2$.* In Figure 10 we show $\chi T$ for $CsNp(SO_4)_2$, where we find negative curvature that extends from 1.8 K to 300 K. This behavior is similar to that of $NaU(SO_4)_2(H_2O)$ and $K_5U_2(SO_4)_6(H_2O)$ and suggests that the crystal electric field splits the degenerate Hund's rule multiplet for the magnetic Np ions, resulting in a reduced effective Np magnetic moment at low temperature. We further note that $\chi T$ approaches 0.8 emu·mol$^{-1}$·K near 300 K, revealing that the full moment of the degenerate multiplet is recovered at higher temperature. This point of view is supported by the behavior of $\chi^{-1}(T)$ (Figure 10 inset), where nearly linear behavior is observed for $T > 100$ K, which can be described by the modified Curie–Weiss expression $\chi(T) = \chi_0 + C/(T - \Theta)$, where $\chi_0 = 0.00026$ emu/mol, $C = 0.93$ emu/mol (in close agreement with expectations from $\chi T$), and $\Theta = -13.5$ K. From the value of $C$, we calculate an effective magnetic moment per Np $\mu_{eff} = 2.72$ $\mu_B$, which is consistent with the Np ions being in the magnetic 3+ (Np 5f$^4$) state. We additionally note that there is no evidence for magnetic ordering at low $T$. In the Figure 10 inset we show $M(H)$ results for $T = 1.8$ K, well within the crystal electric field split ground state. Here, we observe a Brillouin-like magnetic field dependence with a saturation moment of $M_{sat} <$ 0.1 $\mu_B$ /mol, which is strongly reduced from the full Hund's rule multiplet for $Np^{3+}$ $M_{sat} = 2.4$ $\mu_B$/mol. This could simply be due to the crystal electric field splitting. However, this large reduction could also be due to short-range antiferromagnetic interactions as indicated by the large negative Weiss constant.

## CONCLUSIONS

In summary, we showed a new, relatively simple route to air-stable $U^{3+}$ and $Np^{3+}$ products utilizing Zn amalgam and hydrothermal reactions. Starting with the actinyl ions $UO_2^{2+}$ and $NpO_2^{+}$, we produced a family of alkali metal $An^{3+}$ sulfates via *in situ* reduction. The trivalent Np products and the mixed-valent U product were stored exposed to air with no special considerations and have no visible signs of degradation or oxidation after ∼10 months. The other trivalent U products exhibit a thin film of green powder on the crystals after ∼6 months indicating the onset of oxidation. All of the U reactions contained both $U^{3+}$ and $U^{4+}$ except for the reaction containing Na, which produced only a $U^{3+}$ product. Diverging from this, the Np reactions produced only $Np^{3+}$ products. Additionally, only one isotypic product, namely, $NaAn(SO_4)_2(H_2O)$, was common between $U^{3+}$ and $Np^{3+}$. It is unknown whether this difference is from the discrepancy in redox potentials, ionic radii, or some other factor. The Rb congeners of each series represent the only structure types that do not have lanthanide analogues. The *in situ* reduction using Zn amalgam is the same technique we used to prepare the recent Eu(II) borate and exemplifies the robustness of the method. The trivalent state is confirmed by the structures being isotypic to lanthanide compounds, UV–vis–NIR spectra, and magnetic data. While $Np^{3+}$ products have been prepared in the presence of air this is the first report of $U^{3+}$ products being prepared outside of an inert and/or reducing atmosphere.[41,42] The study of magnetic behavior reveals strongly temperature-dependent $\chi T$ values that indicate significant population of excited states at higher temperatures. The short-range antiferromagnetic correlations are much stronger in the mixed-valent $K_5U_2(SO_4)_6(H_2O)$ than in $NaU(SO_4)_2(H_2O)$, but neither of the compounds exhibits magnetic ordering. In general, $Np^{3+}$ magnetism is poorly understood; because it is expected to possess a nonmagnetic singlet ground state, work on 5f$^4$ systems is underdeveloped. We demonstrated that in fact the magnetism is far more complex than anticipated. This work opens up new doors in exploring the chemistry and properties of $U^{3+}$ and $Np^{3+}$. The ease in producing the sulfate complexes, along with their stability in air and water, could prove to be useful as new starting materials for low-valent actinide chemistry.

## ASSOCIATED CONTENT

### Supporting Information

Crystallographic information files, additional crystallographic figures, additional UV–vis–NIR spectra, and photographs of crystals. This material is available free of charge via the Internet at http://pubs.acs.org.

## AUTHOR INFORMATION

### Corresponding Author

*E-mail: albrecht-schmitt@chem.fsu.edu.

### Notes

The authors declare no competing financial interest.

## ACKNOWLEDGMENTS

We are grateful for support provided by the Materials Science of Actinides, an Energy Frontier Research Center funded by the U.S. Department of Energy (DOE), Office of Science (OS), Office of Basic Energy Sciences (OBES) under Award No. DE-SC0001089. A portion of this work was performed at the National High Magnetic Field Laboratory, which is supported by National Science Foundation Cooperative Agreement No. DMR-1157490, the State of Florida, and the U.S. DOE.

## REFERENCES

(1) *The Chemistry of the Actinide and Transactinide Elements;* Edelstein, N. M., Fuger, J., Katz, J. J., Morss, L., Eds.; Springer: Berlin, Germany, 2006; Vol. 3, p 1753.

(2) Krivovichev, S. V.; Burns, P. C. Chapter 1. In *Structural Chemistry of Inorganic Actinides;* Elsevier: Amsterdam, 2007; p 1.

(3) Burns, P. C. *Can. Mineral.* **2005**, *43*, 1839.

(4) Forbes, T. Z.; Wallace, C.; Burns, P. C. *Can. Mineral.* **2008**, *46*, 1623.

(5) Andrews, M. B.; Cahill, C. L. *Chem. Rev.* **2013**, *113*, 1121.

(6) Knope, K. E.; Soderholm, L. *Chem. Rev.* **2013**, *113*, 944.

(7) Macdonald, M. R.; Fieser, M. E.; Bates, J. E.; Ziller, J. W.; Furche, F.; Evans, W. J. *J. Am. Chem. Soc.* **2013**, *135*, 13310.

(8) La Pierre, H. S.; Scheurer, A.; Heinemann, F. W.; Hieringer, W.; Meyer, K. *Angew. Chem., Int. Ed.* **2014**; [Online early access]. DOI: 10.1002/anie.201402050.

(9) Grenthe, I.; Drozdzynski, J.; Fujino, T.; Buck, E. C.; Albrecht-Schmitt, T. E.; Wolf, S. F. *The Chemistry of the Actinide and Transactinide Elements;* Springer: Berlin, Germany, 2006; Vol. *1*, p 253.

(10) Yoshida, Z.; Johnson, S. G.; Kimura, T.; Krsul, J. R. *The Chemistry of the Actinide and Transactinide Elements;* Springer: Berlin, Germany, 2006; Vol. 2, p 699.
(11) Santos, I.; Pires De Matos, A.; Maddock, A. G. *Advances in Inorganic Chemistry;* Sykes, A. G., Ed.; Academic Press, Inc.: San Diego, CA, 1989; Vol. *34*, p 65.
(12) Sorokin, P. P.; Stevenson, M. J. *Phys. Rev. Lett.* **1960**, *5*, 557.
(13) Moro, Fabrizio; Mills, D. P.; Liddle, S. T.; Slageren, J. *Angew. Chem., Int. Ed.* **2012**, *52*, 3430.
(14) Rinehart, J. D.; Long, J. R. *J. Am. Chem. Soc.* **2009**, *131*, 12558.
(15) Rinehart, J. D.; Meihaus, K. R.; Long, J. R. *J. Am. Chem. Soc.* **2010**, *132*, 7572.
(16) Rinehart, J. D.; Long, J. R. *Dalton Trans.* **2012**, *41*, 13572.
(17) Kaltsoyannis, N. *Inorg. Chem.* **2012**, *52*, 3407.
(18) Polinski, M. J.; Grant, D. J.; Wang, S.; Alekseev, E. V.; Cross, J. N.; Villa, E. M.; Depmeier, W.; Gagliardi, L.; Albrecht-Schmitt, T. E. *J. Am. Chem. Soc.* **2012**, *134*, 10682.
(19) Jones, M. B.; Guant, A. J.; Gordon, J. C.; Kaltsoyannis, N.; Neu, M. P.; Scott, B. L. *Chem. Sci.* **2013**, *4*, 1189.
(20) Barnard, R.; Bullock, J. I.; Larkworthy, L. F. *Dalton Trans.* **1972**, 964.
(21) Barnard, R.; Bullock, J. I.; Gellatly, B. J.; Larkworthy, L. F. *Dalton Trans.* **1972**, 1932.
(22) Evans, W. J.; Forrestal, K. J.; Ziller, J. W. *Angew. Chem., Int. Ed.* **1997**, *36*, 774.
(23) Evans, W. J.; Kozimor, S. A.; Ziller, J. W.; Kaltsoyannis, N. *J. Am. Chem. Soc.* **2004**, *126*, 14533.
(24) Evans, W. J.; Traina, C. A.; Ziller, J. W. *J. Am. Chem. Soc.* **2009**, *131*, 17473.
(25) Evans, W. J.; Ziller, J. W.; Kozimor, S. A. *Science* **2005**, *309*, 1835.
(26) Roussel, P.; Scott, P. *J. Am. Chem. Soc.* **1998**, *120*, 1070.
(27) Cloke, F. G. N.; Hitchcock, P. B. *J. Am. Chem. Soc.* **2002**, *124*, 9352.
(28) Fox, A. R.; Bart, S. C.; Meyer, K.; Cummins, C. C. *Nature* **2008**, *455*, 341.
(29) Jones, M. B.; Gaunt, A. J. *Chem. Rev.* **2013**, *113*, 1137.
(30) Drozdzynski, J. *Coord. Chem. Rev.* **2005**, *249*, 2351.
(31) Katz, J. J.; Seaborg, G. T. *The Chemistry of the Actinide Elements;* Pittman Press: Bath, U.K., 1957.
(32) Peretrukhin, V. F.; Krot, N. N.; Gel'man, A. D. *Radiokhimiya* **1966**, *8*, 670.
(33) Barnard, R.; Bullock, J. I.; Larkworthy, L. F. *Chem. Commun.* **1967**, 1271.
(34) Barnard, R.; Bullock, J. I.; Gellatly, B. J.; Larkworthy, L. F. *Dalton Trans.* **1973**, 604.
(35) Bullock, J. I.; King, M. G. *Dalton Trans.* **1975**, 1360.
(36) Apostolidis, C.; Schimmelpfennig, B.; Magnani, N.; Lindqvist-Reis, P.; Walter, O.; Sykora, R.; Morgenstern, A.; Colineau, E.; Caciuffo, R.; Klenze, R.; Haire, R. G.; Rebizant, J.; Bruchertseifer, F.; Fanghanel, T. *Angew. Chem., Int. Ed.* **2010**, *49*, 6343.
(37) Yamamura, T.; Shirasaki, K.; Shiokawa, Y. *J. Phys. Soc. Jpn.* **2006**, *75*, 149.
(38) Schwochau, K.; Drozdzynski, J. *Inorg. Nucl. Chem. Lett.* **1980**, *16*, 423.
(39) Drozdzynski, J.; Schwochau, K.; Schenck, H.-J. *Inorg. Nucl. Chem.* **1981**, *43*, 1845.
(40) Bullock, J. I.; Ladd, M. F. C; Povey, D. C.; Storey, A. E. *Inorg. Chim. Acta* **1980**, *43*, 101.
(41) Gel'man, A. D.; Mefod'eva, M. P. *Atom. Energy* **1958**, *4*, 361.
(42) Mefod'eva, M. P.; Gel'man, A. D. *Sov. Radiochem.* **1971**, *13*, 613.
(43) Krot, N. N.; Mefod'eva, M. P. *Bull. Russ. Acad. Sci.: Phys.* **1974**, *23*, 2052.
(44) Bray, T. H.; Nelson, A.-G. D.; Jin, G. B.; Haire, R. G.; Albrecht-Schmitt, T. E. *Inorg. Chem.* **2007**, *46*, 10959.
(45) Nelson, A.-G. D.; Bray, T. H.; Zhan, W.; Haire, R. G.; Sayler, T. S.; Albrecht-Schmitt, T. E. *Inorg. Chem.* **2008**, *47*, 4945.
(46) Villa, E. M.; Marr, C. J.; Jouffret, L. J.; Alekseev, E. V.; Depmeier, W.; Albrecht-Schmitt, T. E. *Inorg. Chem.* **2012**, *51*, 6548.
(47) Villa, E. M.; Marr, C. J.; Diwu, J.; Alekseev, E. V.; Depmeier, W.; Albrecht-Schmitt, T. E. *Inorg. Chem.* **2013**, *52*, 965.
(48) Aldous, D. W.; Stephens, N. F.; Lightfoot, P. *Dalton Trans.* **2007**, 4207.
(49) Manos, M. J.; Kanatzidis, M. G. *Inorg. Chem.* **2009**, *48*, 4658.
(50) Belai, N.; Frisch, M.; Ilton, E. S.; Ravel, B.; Cahill, C. L. *Inorg. Chem.* **2008**, *47*, 10135.
(51) Chen, C.-S.; Lee, S.-F.; Lii, K.-H. *J. Am. Chem. Soc.* **2005**, *127*, 12208.
(52) Lin, C.-H.; Chen, C.-S.; Shiryaev, A. A.; Zubavichus, Y. V.; Lii, K.-H. *Inorg. Chem.* **2008**, *47*, 4445.
(53) Nguyen, Q. B.; Chen, C.-L.; Chiang, Y.-W.; Lii, K.-H. *Inorg. Chem.* **2012**, *51*, 3879.
(54) Lin, C.-H.; Lii, K.-H. *Angew. Chem., Int. Ed.* **2008**, *47*, 8711.
(55) Lee, C.-S.; Wang, S.-L.; Lii, K.-H. *J. Am. Chem. Soc.* **2009**, *131*, 15116.
(56) Lee, C.-S.; Lin, C.-H.; Wang, S.-L.; Lii, K.-H. *Angew. Chem., Int. Ed.* **2010**, *49*, 4254.
(57) Nguyen, Q. B.; Liu, H.-K.; Chang, W.-J.; Lii, K.-H. *Inorg. Chem.* **2011**, *50*, 4241.
(58) Yeon, J.; Smith, M. D.; Sefat, A. S.; Tran, T. T.; Halasyamani, P. S.; zur Loye, H.-C. *Inorg. Chem.* **2013**, *52*, 8303.
(59) Sheldrick, G. M. *Acta Crystallogr.* **2008**, *A64*, 112.
(60) Sheldrick, G. M. *SADABS, Program for absorption correction using SMART CCD based on the method of Blessing;* Bruker AXS: Madison, WI, 2001.
(61) Blessing, R. H. *Acta Crystallogr.* **1995**, *A51*, 33.
(62) Sheldrick, G. M. *Acta Crystallogr.* **2008**, *A64*, 112.
(63) Spek, A. L. *J. Appl. Crystallogr.* **2003**, *36*, 7.
(64) Lindgren, O. *Acta Chem. Scand., Ser. A* **1977**, *31*, 591.
(65) Blackburn, A. C.; Gerkin, R. E. *Acta Crystallogr.* **1995**, *C51*, 2215.
(66) Perles, J.; Fortes-Revilla, C.; Gutierrez-Puebla, E.; Iglesias, M.; Monge, M. A.; Ruiz-Valero, C.; Snejko, N. *Chem. Mater.* **2005**, *17*, 2701.
(67) Wu, C.-D.; Liu, Z.-Y. *J. Solid State Chem.* **2006**, *179*, 3500.
(68) Kazmierczak, K.; Hoeppe, H. A. *J. Solid State Chem.* **2010**, *183*, 2087.
(69) Tursina, A. I.; Iskhakova, L. D. *Zh. Strukt. Khim.* **1987**, *30*, 135.
(70) Casari, B. M.; Langer, V. *Z. Anorg. Allg. Chem.* **2007**, *633*, 1055.
(71) Bukovec, N.; Kaucic, V.; Golic, L. *Acta Crystallogr.* **1980**, *B36*, 129.
(72) Degtiarev, P. A.; Pokrovskii, A. N.; Kova, L. M.; Korytnaia, F. M. *J. Solid State Chem.* **1977**, *22*, 419.
(73) Gorden, A. E. V.; Xu, J.; Raymond, K. N. *Chem. Rev.* **2003**, *103*, 4207.
(74) Kepert, D. L. *Prog. Inorg. Chem.* **1978**, *24*, 179.
(75) Bukovec, N.; Golic, L.; Bukovec, P.; Siftar, J. *Monatsch. Chem.* **1978**, *109*, 1305.
(76) *Lanthanide and Actinide Chemistry;* Fields, P. R., Moeller, T., Eds.; Advances in Chemistry Series No. 71; American Chemical Society: Washington, D.C., 1967; 86.
(77) Cohen, D.; Carnall, W. T. *J. Phys. Chem.* **1960**, *12*, 1933.
(78) Carnall, W. T.; Crosswhite, H. M.; Pappalardo, R. G.; Cohen, D.; Fried, S. *J. Chem. Phys.* **1974**, *61*, 4993.
(79) Krupke, W. F.; Gruber, J. B. *J. Chem. Phys.* **1967**, *46*, 542.